

Synthesis of a Hydroxyapatite Nanopowder via Ultrasound Irradiation from Calcium Hydroxide Powders for Potential Biomedical Applications

Sridevi Brundavanam, G errard Eddy Jai Poinern^{*}, Derek Fawcett

Murdoch Applied Nanotechnology Research Group, Department of Physics, Energy Studies and Nanotechnology, School of Engineering and Energy, Murdoch University, Australia

Copyright   2015 Horizon Research Publishing All rights reserved.

Abstract Nanoscale hydroxyapatite based ceramics are a relatively new form of materials that are currently being investigated for a number of potential biomedical applications. This study reports on a straightforward wet chemical method that uses calcium hydroxide and phosphoric acid as precursors. After chemical synthesis a conventional thermal treatment was used to produce an ultrafine hydroxyapatite nanopowder. Varying ultrasonic power between zero and 400 W during the synthesis process produced crystallite sizes ranging from 15.4 nm down to 12.2 nm. The morphology of particles synthesized under the influence of ultrasonic irradiation was predominantly spherical and granular. Also present were a small number of irregular shaped plates. Energy dispersive spectroscopy revealed the samples had a Ca:P ratio of 1.66, which was very close to the ideal value of 1.67. FT-IR studies identified functional groups and confirmed the results of the X-ray diffraction data that the powders were indeed composed of nanoscale hydroxyapatite.

Keywords Hydroxyapatite, Biomaterials, Nanometer Scale Materials, Ultrasound

1. Introduction

The efficient repair of hard tissues that form the human skeletal system continues to be a challenging goal in biomedical engineering. For many years, a variety of biologically compatible ceramics such as alumina, bioactive glasses, calcium phosphates and zirconia have been used in reconstructive and regenerative hard tissue procedures with varying degrees of success [1-3]. Importantly, any ceramic being considered for a biomedical application must be completely biologically compatible. Specifically, it must be biologically stable [4], nontoxic and non-immunogenic to body tissues [5, 6]. Among the biologically compatible ceramics, calcium phosphates are compositionally similar to

the mineral phase found in bone and consequently have been used in a variety of bone replacement therapies [7, 8]. Besides being compositionally similar, calcium phosphates are lightweight, chemical stable and are composed of ions commonly found in physiological environment [9]. The two most studied and used forms of calcium phosphates in the biomedical field are tri-calcium phosphate [$\text{Ca}_3(\text{PO}_4)_2$, TCP] and hydroxyapatite [$\text{Ca}_{10}(\text{OH})_2(\text{PO}_4)_6$, HAP]. For example, HAP is ideal for many biomedical applications since it is the most thermodynamically stable calcium phosphate in the physiological environment [10]. Furthermore, studies have shown that HAP has good biocompatibility and bioactive properties with body tissues. In particular, for bone tissue engineering applications it offers good osteoconductivity and osteoinductivity capabilities. While its slow biodegradability in situ allows tissue regeneration and tissue replacement to take place [3, 11, 12]. These properties are of particular importance since bone continually undergoes cellular remodeling and as a result tissue is simultaneously deposited by osteoblasts cells and removed by osteoclasts cells [3, 13]. It is due to the advantageous bioactive properties of HAP that has made it a successful biomaterial for a number of clinical applications such as dental repair procedures, repairing bone defects, bone augmentation and coatings on metallic implants [14, 15]. The positive results achieved in these clinical applications has encouraged further research into HAP and its potential use in a variety of new tissue regeneration and tissue engineering applications [16, 17]. To date several ceramic processing techniques have been used to synthesize HAP such as wet precipitation, sol-gel, hydrothermal and ultrasonic [18-22]. However, there is a current need to develop more efficient processing techniques that have the potential to deliver large quantities of HAP nanopowders for future biomedical applications.

In the present study, a straightforward synthesis process was used to precipitate HAP seeds from a solution containing calcium hydroxide and phosphoric acid. The process was conducted at room temperature, while the solution pH was maintained at 10 via the addition of

ammonia. Synthesis was carried out with and without ultrasonic irradiation to examine its influence on particle size and morphology. After a straightforward thermal treatment, particle size, composition, crystalline structure and morphology of nanopowders were studied using advanced characterization techniques such as powder X-ray diffraction (XRD) spectroscopy, Field Emission Scanning Electron Microscopy (FESEM), Energy Dispersive Spectroscopy (EDS) and Fourier Transform Infrared spectroscopy (FT-IR).

2. Materials and Methods

2.1. Materials

HAP powders were synthesised from analytical grade calcium hydroxide [$\text{Ca}(\text{OH})_2$] supplied the source of Ca^{2+} ions and analytical grade phosphoric acid [H_3PO_4 (86.2%)] supplied the source of phosphate ions. Calcium hydroxide was purchased from Ajax Finechem (New South. Wales, Australia) and phosphoric acid was purchased from Fisher Scientific (Fair Lawn, NJ, USA). Solution pH was achieved by the addition of ammonia that was supplied by CHEM-SUPPLY (New South Wales, Australia). All aqueous solutions were made using Milli-Q[®] water (18.3 $\text{M}\Omega \text{ cm}^{-1}$) produced by an ultrapure water system (Barnstead Ultrapure Water System D11931; Thermo Scientific, Dubuque, IA). The ultrasound processor used

during ultrasonic assisted synthesis of HAP powders was an UP400S [400 W, 24 kHz, H22 Sonotrode (22 mm diameter, 45 mm maximum submerged depth)] supplied by Hielscher Ultrasonic Technology. Ultrasonic outputs were controlled by operating the rotary regulator as per the manufacturer's specifications (20% to 100%).

2.2. Synthesis of Nanometre Scale HAP Powders

The synthesis procedure begins by preparing a 100 mL aqueous solution of 0.32M $\text{Ca}(\text{OH})_2$ in a glass beaker. The solution was then heated to 40 °C under vigorous stirring for 15 minutes on a standard laboratory hotplate/magnetic stirrer. Then a 100 mL solution of 0.19 M H_3PO_4 was slowly added to the $\text{Ca}(\text{OH})_2$ solution. The mixture was further stirred for 15 minutes while the mixture pH was adjusted to 10 by the drop-wise addition of ammonia. At the end of the mixing period, excess fluid was decanted from the beaker and the precipitate was deposited onto a glass dish. The dish was then placed onto a hotplate which was progressively heat up to 300 °C. The precipitate was then thermally treated for 3 h. The synthesis procedure is schematically presented in Figure 1 (a). Ultrasonically assisted synthesis follows a similar procedure except for two 30 minutes ultrasonic treatment periods as indicated in the schematic procedure presented in Figure 1 (b). At the end of each synthesis procedure the resulting powders were examined using advanced characterisation techniques.

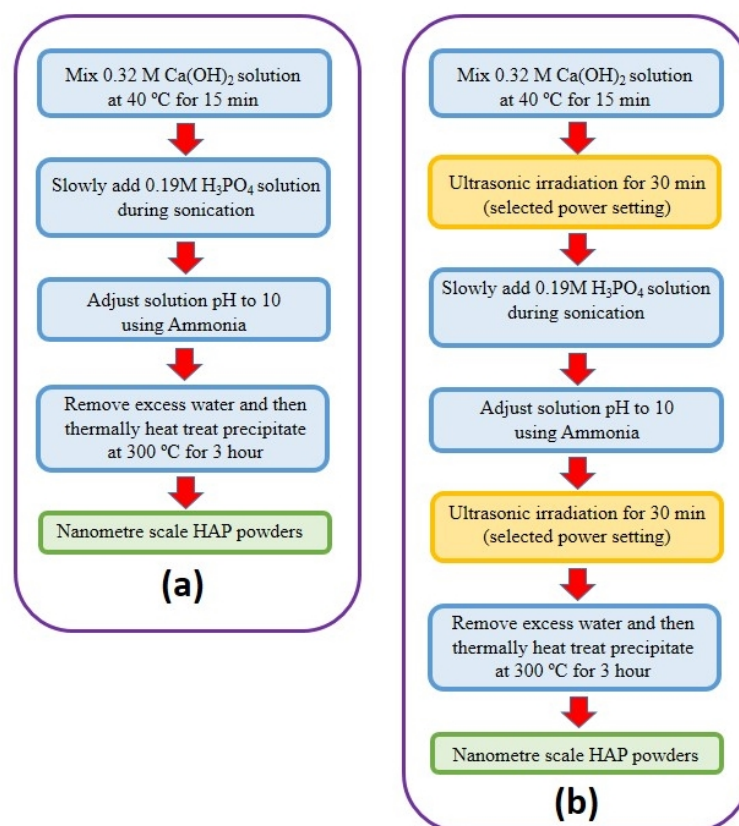


Figure 1. Schematic of experimental procedures used for synthesizing HAP nanopowders: (a) without ultrasound and (b) with ultrasound

2.3. Advanced Characterisation

2.3.1. Powder X-ray Diffraction (XRD) Spectroscopy

X-ray diffraction (XRD) spectroscopy was used to study the phase's present and crystalline sizes in the powder samples. Spectroscopy data was recorded at room temperature, using a GBC[®] eMMA X-ray Powder Diffractometer [Cu K α = 1.5406 Å radiation source] operating at 35 kV and 28 mA. The diffraction patterns were collected over a 2θ range of 20° to 60° with an incremental step size of 0.02° using flat plane geometry with 2 second acquisition time for each scan.

2.3.2. Transmission Electron Microscopy (TEM)

The size and morphology of particles formed by the synthesis process were investigated using TEM. Sample preparation consisted of collecting a portion of the synthesized powder and then placing it into a small tube containing Milli-Q[®] water. The tubes were then sealed and placed into an ultrasonic bath for 10 minutes. Then a single drop from the suspension was deposited onto a carbon-coated copper TEM grid using a micropipette and then allowed to slowly dry over a 24-hour period. After sample preparation a bright field TEM study was carried out using a Phillips CM-100 electron microscope (Phillips Corporation Eindhoven, The Netherlands) operating at 80kV. TEM was also used in conjunction with FESEM images to measure particle sizes and determine particle morphology

present in the powders samples.

2.3.3. Fourier Transform Infrared Spectroscopy (FT-IR)

Fourier transform infrared spectra (FT-IR) spectroscopy was used to identify species, functional groups and vibration modes present in the respective powder samples. Powder analysis was carried out using a Perkin-Elmer Frontier FT-IR spectrometer with Universal Single bounce Diamond ATR attachment. FT-IR spectra were recorded in the range from 525 to 4000 cm^{-1} in steps of 4 cm^{-1} .

2.3.4. Field Emission Scanning Electron Microscopy (FESEM) and Energy Dispersive Spectroscopy (EDS)

All micrographs were taken using a FE-SEM Zeiss Neon 40 EsB with an attached energy dispersive X-ray spectrometer. The micrographs were used to study the size, shape and morphological features of the synthesized powders. Samples were mounted on individual substrate holders using carbon adhesive tape before being sputter coated with a 2 nm layer of platinum to prevent charge build up using a Cressington 208HR High Resolution Sputter coater. The EDS technique was used to verify the results of the XRD analysis and to calculate the Ca/P ratio of the synthesized powders. In addition, FESEM was also used in conjunction with TEM images to measure particle sizes and determine particle morphology present in the powders samples.

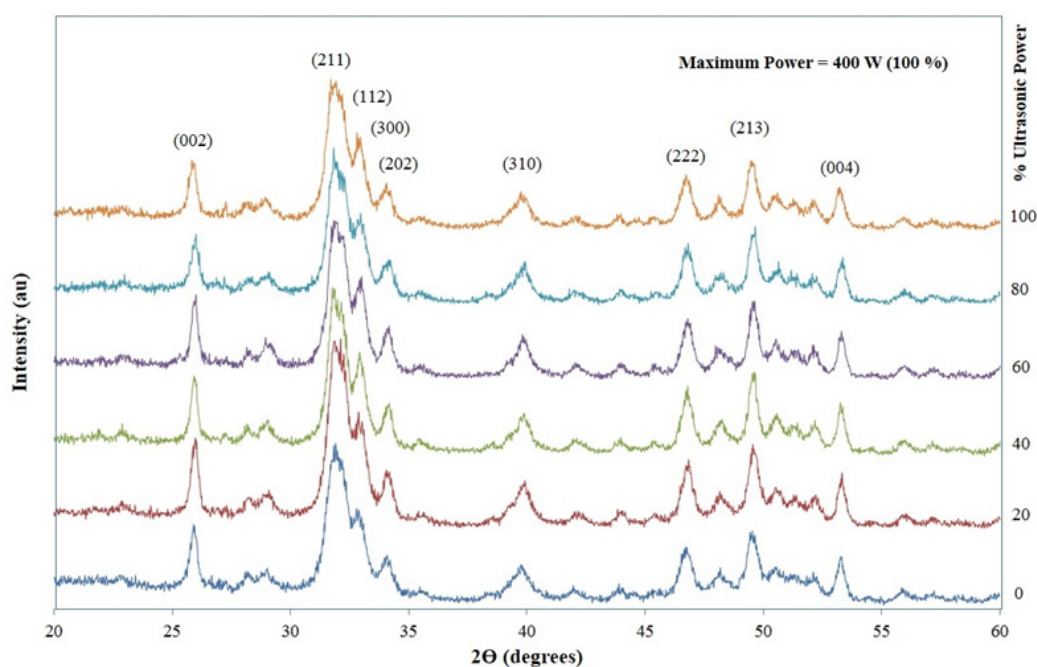


Figure 2. XRD patterns of nanometre scale hydroxyapatite powders synthesized under the influence of ultrasonic irradiation ranging from 0 to 400 W.

3. Results and Discussions

3.1. XRD Spectroscopy and TEM Analysis

Analysis of powder XRD patterns was used to identify the purity and crystalline size of HAP nanopowders produced with and without ultrasonic power. Figure 2 presents representative XRD patterns for nanopowder samples. Maximum ultrasonic power used was 400 W (100 %) and lower power level measurements were carried out at pre-determined power levels (0 %, 20 %, 40 %, 60 %, 80 % and 100 %). All patterns in Figure 2 match the known phases for pure HAP and are consistent with the phases listed in the ICDD database. In addition, each pattern identifies the main (h k l) indices associated with peaks found in the HAP samples, namely (002), (211), (300), (202), (310), (222) and (213). All patterns show characteristic HAP peaks and no evidence of non-HAP related phases were seen. Further analysis was carried out to determine the crystalline size, $t_{(hkl)}$, of each powder sample using the Debye-Scherrer equation [23-25].

$$t_{(hkl)} = \frac{0.9\lambda}{B \cos\theta_{(hkl)}} \quad (1)$$

where, λ is the wavelength of the monochromatic X-ray beam, B is the Full-Width at Half Maximum (FWHM) of the peak at the maximum intensity, $\theta_{(hkl)}$ is the peak diffraction angle that satisfies Bragg's law for the (h k l) plane and $t_{(hkl)}$ is the crystallite size. The crystallite size for each sample was calculated from the (002) reflection peak. Analysis of crystallite size data revealed increasing ultrasonic power tended to produce smaller crystallite sizes. Synthesis of powders without ultrasound power gave a mean value of 15.4 nm and powders synthesized at 400 W produced crystallites with a mean value of 12.2 nm as seen in Figure 4 (a).

Figure 3 (a) presents a representative TEM image of $\text{Ca}(\text{OH})_2$ particles prior to synthesis. The particles are

spherical and range in size from 0.1 μm up to 0.3 μm . Figure 3 (b) presents a typical image of HAP powders produced without the presence of ultrasonic power. The particles are rod-like to needle-like in shape and indicate growth in the c direction. The particles tend to be around 10 nm in diameter, but range in length from 50 nm upwards. However, this is not the case for powders synthesized under the influence of ultrasonic irradiation as seen in Figure 4 (b). The TEM image shows a completely different particle size and morphology. The morphology is predominantly spherical and granular in nature, but present were a small number of irregular shaped platelets which can also be seen in the high resolution FESEM image presented in Figure 4 (c).

3.2. FESEM, EDS and FTIR Spectroscopy

FESEM in conjunction with TEM microscopy was used to study particle size and morphology of nanopowders synthesized under the influence ultrasonic irradiation. Both Figure 4 (b) and (c) reveal the powder sample synthesized at 400 W is highly agglomerated. The particle morphology seen in this study is similar to morphologies previously reported in the literature [22-25]. Particle size analysis based on TEM and FESEM images for the 400 W power setting reveals a narrow particle size distribution. Particle sizes range from 20.0 nm up 66.7 nm, with spherical particles having a mean diameter of 22.8 nm and granular particles having a mean diameter of 36.7 nm as seen in Table 1. Close examination of Figure 4 (c) also reveals the presence of a small number of tube-like and irregular shaped platelets. Both of these particle features are within the narrow particle distribution as indicated in Table 1. This narrow particle distribution has also been seen in similar studies involving the sonochemical synthesis of HAP [26]. Figure 4 (d) presents a EDS spectrum of a typical powder sample showing peaks corresponding to Ca, P, and O. The presence of these peaks confirms the chemical composition of HAP. Analysis of EDS data indicated that the powder had a Ca:P ratio of 1.66, which was very close to the ideal value of 1.67.

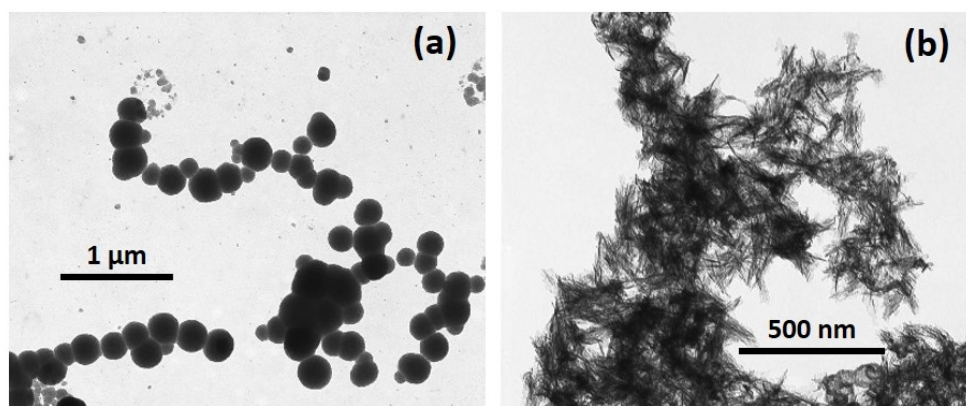


Figure 3. (a) TEM image of $\text{Ca}(\text{OH})_2$ particles prior to synthesis and (b) representative TEM image of HAP synthesized without ultrasonic irradiation.

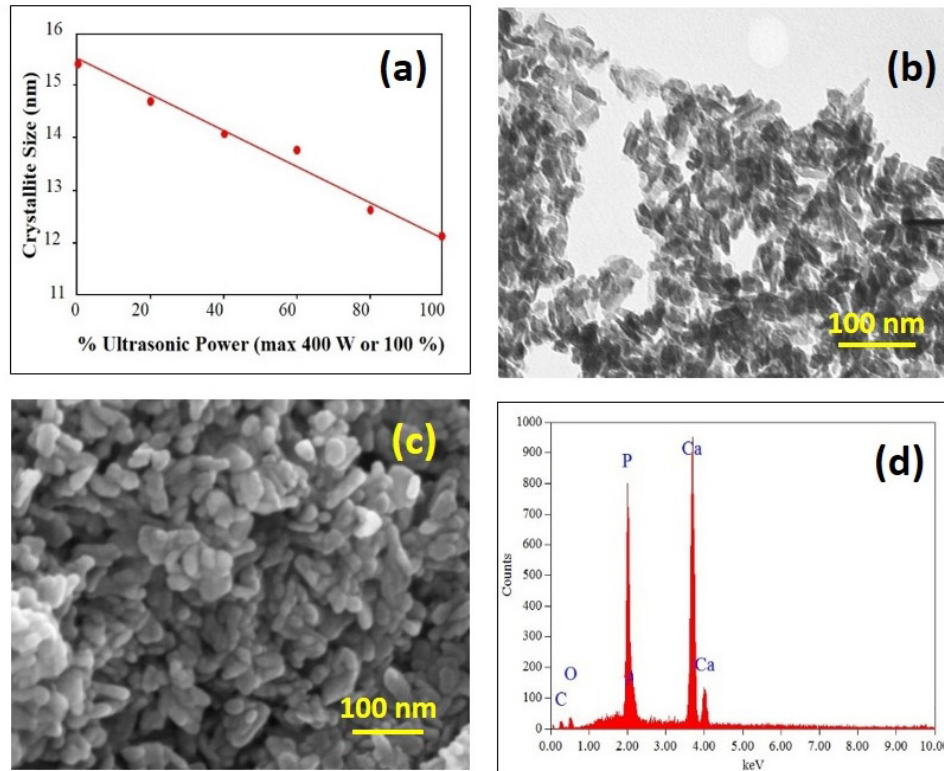


Figure 4. (a) Graphical results of XRD analysis showing the crystallite size dependence on ultrasonic power used during synthesis, Representative TEM micrograph (b) and high resolution FESEM (c) showing the spherical and granular shaped HAP particles synthesized.

Table 1. Particle size distribution and morphology from TEM and FESEM analysis for a HAP nanopowder synthesized under the influence of 400 W.





Shape	Profile	Size Range (nm)	Aspect Ratio	Mean (nm)	Std. Dev. (nm)	% of Sample
Spherical (smooth)	Dia. 	20.0 – 33.4	NA	22.8	3.7	44.9
Spherical (angular)	Dia. 	26.7 – 46.7	NA	36.7	7.5	26.1
Irregular	Width Length 	20.0 – 40.2	1:7	27.4	7.4	17.4
		33.4 – 66.7		47.3	4.8	
Rod like	Dia. Length 	20.0 – 33.3	1:2	21.7	4.4	11.6
		40.0 – 66.7		43.4	8.8	
Total						100.0

Figure 5 presents representative FT-IR spectra of three HAP nanopowders synthesized under various levels of ultrasonic irradiation. The first spectrum (Blue) is a powder synthesized without ultrasonic irradiation. The other two spectra are powders synthesized under different ultrasonic power levels [Red (80 W ~ 20 %) and Green (400 W ~ 100 %)]. All three spectra have similar band locations and intensities normally associated with nanoscale HAP. Considering all three spectra together, starting from the right hand side of Figure 5 and moving to the left the various bands are identified. The first two bands encountered are 562 cm^{-1} and 601 cm^{-1} , which are the result of ν_4 vibrations produced by the O-P-O mode. The next significant bands located at 631 cm^{-1} and 880 cm^{-1} are associated with the carbonate groups and clearly indicate the presence of carbonates in all three sample spectra. The next band located at 964 cm^{-1} is the result of ν_1 symmetric stretching vibrations

normally associated with the P-O mode.

The very strong bands located at 1024 cm^{-1} and 1090 cm^{-1} indicated the presence of PO_4^{3-} functional groups (P-O mode) and the weaker bands at 1415 cm^{-1} and 1460 cm^{-1} corresponds to CO_3^{2-} functional groups. The next band located at 1654 cm^{-1} also corresponds to a CO_3^{2-} group. The presence of carbonates in the samples most likely results from atmospheric carbon dioxide interacting with the alkaline HAP precursor solution during the synthesis process [27-29]. The band located at 2978 cm^{-1} indicates the stretching vibrations associated with the C-H mode, while the band located at 3376 cm^{-1} indicates the presence of absorbed water. The final peak located at 3569 cm^{-1} corresponds to OH^- vibrations in the HAP lattice. The results of the FT-IR analysis have clearly identified functional groups normally associated with HAP and confirm the results of the XRD data.

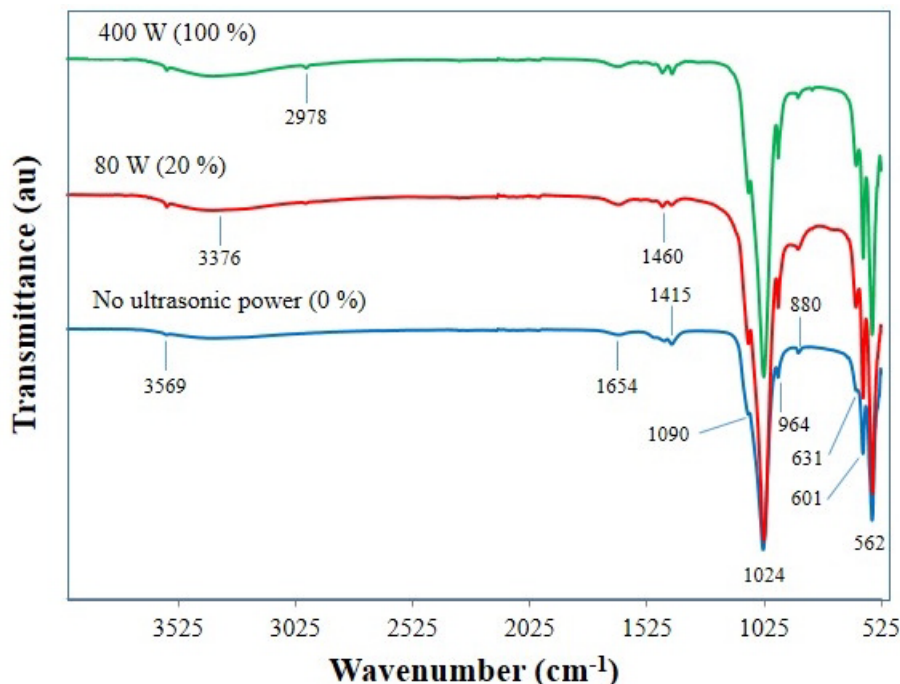


Figure 5. FT-IR spectroscopy analysis of representative synthesized hydroxyapatite powders produced under the influence of ultrasonic irradiation.

The results of the study have shown that synthesis of nanoscale HAP from an aqueous solution containing calcium hydroxide and phosphoric acid without the aid of ultrasonic irradiation produced particles with a needle-like morphology. However, aqueous solutions subjected to ultrasonic irradiation during synthesis tended to produce a different particle size and morphology. Ultrasound assisted synthesis produced particles with a morphology that was predominantly spherical and granular in nature. Also present in the samples were a small number of irregular shaped platelets. The particle size distribution was narrow and ranged from 20.0 nm up 66.7 nm. Both XRD and FT-IR characterization studies confirmed the powders were nanoscale HAP. Further studies are needed to examine the influence of higher ultrasonic powers above the 400 W power level used in this method. The advantage of this method is its simple and straightforward set-up, and its potential scale-up capability for the production of larger powder quantities. The next stage in the research is to investigate the biological compatibility of the HAP produced using this method via *in vitro* studies using bone cells.

4. Conclusions

The results of the study have shown that a straightforward wet chemical method using calcium hydroxide and phosphoric acid as precursors was capable of producing HAP nanopowders. The use of ultrasonic irradiation during synthesis leads to the formation of nanoscale HAP powders with a relatively narrow size distribution. Particles produced were predominantly spherical and granular ranging in size from 20.0 nm up to 66.7 nm. There were also smaller numbers of small platelets seen in the FESEM and TEM

images. XRD studies revealed powders synthesized without ultrasonic irradiation produced a mean crystallite size of around 15.4 nm. Varying ultrasonic power from zero to 400 W produced crystallites ranging in size from 15.4 nm down to 12.2 nm. Analysis of the EDS data established a Ca:P ratio of 1.66, which was very close to the ideal value of 1.67. FT-IR studies were used to categorize functional groups present in the samples and confirmed XRD studies identifying the samples as nanoscale HAP. The study has shown that ultrasonic irradiation played an important role in determining crystallite size, particle size and particle morphology. However, further studies are needed to examine the influence of larger ultrasonic powers using this method and biological compatibility studies via *in vitro* cell studies needs to be undertaken.

Acknowledgements

Mrs. Sridevi Brundavanam would like to acknowledge Murdoch University for providing her PhD Scholarship to undertake the hydroxyapatite synthesis studies as part of her PhD project.

REFERENCES

- [1] A. El-Ghannam, Bone reconstruction: from bioceramics to tissue engineering, *Expert. Rev. Med. Devices*, Vol. 2, No. 1, 87-101, 2005.
- [2] S. Oh, N. Oh, M. Appleford, J. L. Ong, Bioceramics for tissue engineering applications: A review, *American Journal of*

- Biochemistry and Biotechnology. Vol. 2, No. 2, 49-56, 2006.
- [3] G. E. J. Poinern, R. Brundavanam, X. Le, P. K. Nicholls, M. A. Cake, D. Fawcett, The synthesis, characterisation and in vivo study of a bioceramic for potential tissue regeneration applications, *Scientific Reports*, Vol. 4, No. 6235, 1-9, 2014.
- [4] C. Song, et al., Facilitation of hematopoietic recovery by bone grafts with intra-bone marrow-bone marrow transplantation, *Immunobiology*, Vol. 213, 455-468, 2008.
- [5] O. S. Schindler, et al., Use of a novel bone graft substitute in peri-articular bone tumours of the knee, *The Knee*, Vol. 14, 458-464, 2007.
- [6] R. Murugan, S. Ramakrishna, Development of nanocomposites for bone grafting, *Comp. Sci. Technol.*, Vol. 65, 2385-2406, 2005.
- [7] D. W. Huttmacher, J. T. Schantz, C. X. F. Lam, K. C. Tan, T. C. Lim, State of the art and future directions of scaffold-based bone engineering from a biomaterials perspective, *J. Tissue Eng. Regen. Med.*, Vol. 1, 245-260, 2007.
- [8] W. J. E. M. Habraken, J. G. C. Wolke, J. A. Jansen, Ceramic composites as matrices and scaffolds for drug delivery in tissue engineering, *Advanced Drug Delivery Reviews*, Vol. 59, 234-248, 2007.
- [9] S. V. Dorozhkin, Nanodimensional and nanocrystalline apatites and other calcium orthophosphates in biomedical engineering, biology and medicine. *Materials*, Vol. 2, 1975-2045, 2009.
- [10] S. J. Kalita, A. Bhardwaj, H. A. Bhatt, Nanocrystalline calcium phosphate ceramics in biomedical engineering, *Materials Science and Engineering C*, Vol. 27, No. 3, 441-449, 2007.
- [11] A. Blom, Which scaffold for which application? *Current Orthopaedics*, Vol. 21, No. 4, 280-287, 2007.
- [12] P. Habibovic, K. de Groot, Osteoinductive biomaterials-properties and relevance in bone repair, *J. Tissue Eng and Regen Med.*, Vol. 1, 25-32, 2007.
- [13] X. Luo, et al., Zinc in calcium phosphate mediates bone induction: in vitro and in vivo model, *Acta Biomaterialia*, Vol. 10, 477-485, 2014.
- [14] S. T. Kao, D. D. Scott, Review of Bone Substitutes. *Oral. Maxillofac. Surg. Clin. North Am.*, Vol. 19, 513-521, 2007.
- [15] E. Cunningham, et al., High solid content hydroxyapatite slurry for the production of bone substitute scaffolds, *Proc. IMechE. HJ. Eng. Med.*, Vol. 223, 727-737, 2009.
- [16] M. Epple, et al., Application of calcium phosphate nanoparticles in biomedicine, *J. Mater.Chem.* Vol. 20, 18-23, 2010.
- [17] D. Hagemeyer, et al., Self-assembly of calcium phosphate nanoparticles into hollow spheres induced by dissolved amino acids. *J. Mater. Chem.*, Vol. 21, 9219-9223, 2011.
- [18] M. R. Saeri, et al., The wet precipitation process of hydroxyapatite. *Mater. Lett.*, Vol. 57, 4064-4069, 2003.
- [19] A. Afshar, et al., Some important factors in the wet-precipitation process of hydroxyapatite. *Materials and Design*. Vol. 24, 197-202, 2003.
- [20] G. Bezzi, et al., A novel sol-gel technique for hydroxyapatite preparation. *Materials Chemistry and Physics*. Vol. 78, 816-824, 2003.
- [21] Y. Wang, et al., Hydrothermal synthesis of hydroxyapatite nano-powders using cationic surfactant as a template. *Mater. Lett.*, Vol. 60, 1484-1487, 2006.
- [22] G. E. J. Poinern, et al., Thermal and ultrasonic influence in the formation of nanometre scale hydroxyapatite bio-ceramic. *International Journal of Nanomedicine*, Vol. 6, 2083-2095, 2011.
- [23] H. P. Klug, L. E. Alexander, X-ray diffraction procedures for poly-crystallite and amorphous materials, Wiley, New York, 1974.
- [24] C. S. Barrett, J. B. Cohen, J. Faber, J. R. Jenkins, D. E. Leyden, J. C. Russ, P. K. Predecki, *Advances in X-ray analysis*, Vol. 29, Plenum Press, New York, 1986.
- [25] S. N. Danilchenko, O. G. Kukhareenko, C. Moseke, I. Y. Protsenko, L. F. Sukhodub, B. Sulkio-Cleff, Determination of the bone mineral crystallite size and lattice strain from diffraction line broadening, *Cryst. Res. Technol.*, Vol. 37, 1234-1240, 2002.
- [26] W. Kim, F. Saito, Sonochemical synthesis of hydroxyapatite from H₃PO₄ solution with Ca(OH)₂, *Ultrasonics Sonochemistry*, Vol. 8, 85-88, 2001.
- [27] R. N. Panda, et al., FTIR, XRD, SEM and solid state NMR investigations of carbonate-containing hydroxyapatite nano-particles synthesised by hydroxide-gel technique, *J. Physics and Chemistry of Solids*, Vol. 64, 193-199, 2003.
- [28] Y. Wang, et al., Surfactant-assisted synthesis of hydroxyapatite particles. *Mater. Lett.*, Vol. 60, 3227-3231, 2006.
- [29] Y. Wang, et al., Hydrothermal synthesis of hydroxyapatite nano-powders using cationic surfactant as a template. *Mater. Lett.*, Vol. 60, 1484-1487, 2006.